

Paraspeckles interact with SWI/SNF subunit ARID1B to regulate transcription and splicing

Divya Reddy, Saikat Bhattacharya , Michaella Levy, Ying Zhang, Madelaine Gogol, Hua Li, Laurence Florens & Jerry L Workman* 

Abstract

Paraspeckles are subnuclear RNA–protein structures that are implicated in important processes including cellular stress response, differentiation, and cancer progression. However, it is unclear how paraspeckles impart their physiological effect at the molecular level. Through biochemical analyses, we show that paraspeckles interact with the SWI/SNF chromatin-remodeling complex. This is specifically mediated by the direct interaction of the long-non-coding RNA NEAT1 of the paraspeckles with ARID1B of the cBAF-type SWI/SNF complex. Strikingly, ARID1B depletion, in addition to resulting in loss of interaction with the SWI/SNF complex, decreases the binding of paraspeckle proteins to chromatin modifiers, transcription factors, and histones. Functionally, the loss of ARID1B and NEAT1 influences the transcription and the alternative splicing of a common set of genes. Our findings reveal that dynamic granules such as the paraspeckles may leverage the specificity of epigenetic modifiers to impart their regulatory effect, thus providing a molecular basis for their function.

Keywords chromatin; lncRNA; paralogs; phase separation; transcription

Subject Categories Chromatin, Transcription & Genomics

DOI 10.15252/embr.202255345 | Received 3 May 2022 | Revised 12 October 2022 | Accepted 20 October 2022 | Published online 10 November 2022

EMBO Reports (2023) 24: e55345

Introduction

Membrane-less organelles are phase-separated structures that can be found in different physiological contexts inside the cell (Gomes & Shorter, 2019). In addition to organizing and concentrating proteins, they are believed to fine-tune biochemical processes such as transcription and splicing (Gomes & Shorter, 2019; Zhang & Rabouille, 2019). They are also physiologically important as structures such as the P-bodies have been shown to be required for fertility in adults, while neuronal granules enable a time- and space-dependent mRNA expression that is critical for neuronal activity (Formicola *et al.*, 2019; Marnik & Updike, 2019).

Paraspeckles are one such membrane-less organelles in the interchromatin space of mammalian cell nuclei (Fox *et al.*, 2002). They

are formed primarily by the association of long-non-coding RNAs (lncRNAs) and numerous RNA-binding proteins (Fox *et al.*, 2005). The core paraspeckle components include the RNA-binding paraspeckle proteins (PSPs) such as PSPC1, SFPQ, and NONO, and the lncRNA and nuclear enriched abundant transcript 1 (NEAT1; also known as nuclear paraspeckle assembly transcript 1; Naganuma *et al.*, 2012). There are two isoforms of NEAT1, NEAT_1 and NEAT_2, both of which are expressed in various differentiated mammalian cells. Both the isoforms are part of the paraspeckles, however, NEAT1_2 is an essential architectural component of these granules (Kawaguchi & Hirose, 2012; Butler *et al.*, 2019). Assembly of these nuclear granules occurs as soon as the NEAT1 RNA starts emerging from its synthesis site and is bound by the PSPs (Clemson *et al.*, 2009; Isobe *et al.*, 2020). However, NEAT1 accumulation on its own is insufficient for paraspeckle formation (Naganuma *et al.*, 2012). This suggests that the protein components of the paraspeckles are required for its formation. Interestingly, these proteins, although enriched in paraspeckles, are not exclusively localized in them and have a broad nucleoplasmic distribution (Hirose *et al.*, 2014). Therefore, the PSPs are believed to be exchanged dynamically between the paraspeckles and the nucleoplasm through diffusion (Fox *et al.*, 2018).

Paraspeckles have gained interest in recent times as they have been implicated in the regulation of transcription and alternative splicing (AS) as well as translation inhibition (Anantharaman *et al.*, 2016; Pisani & Baron, 2019; Li & Wang, 2021). They were initially thought to be functionally dispensable as NEAT1 knockout mice are viable and fertile (Nakagawa *et al.*, 2011). However, subsequent studies have revealed that they are important during the development of the corpus luteum and the mammary gland in mice (Nakagawa *et al.*, 2014; Standaert *et al.*, 2014). Paraspeckles also have been shown to alter in size and nuclear distribution in response to various environmental cues including stresses such as virus infection, DNA damaging agents, and differentiation signals (Adriaens *et al.*, 2016, 2019; Wang *et al.*, 2020). Physiologically, this makes them important as they are involved in diseases such as cancer and neurodegeneration (An *et al.*, 2018; Pisani & Baron, 2020). Yet, how these structures impart their function to affect the wide-ranging cellular processes largely remains unclear. This has been especially challenging to address as paraspeckles have numerous protein components such as the HNRNPs, SRSFs,

and RBPs that are known to exist independent of paraspeckles and are not essential for their integrity (An *et al*, 2019). Therefore, a better understanding of what the paraspeckles engage with as a complex may shed light on the molecular basis of their function.

Switch/sucrose non-fermentable (SWI/SNF), also known as brahma associated factors (BAF), is an ATP-dependent chromatin-remodeling complex that is highly conserved across different organisms (Kadoch & Crabtree, 2015). It makes the underlying DNA sequence within the chromatin accessible to cellular machinery by altering nucleosome occupancy by using energy derived from ATP hydrolysis (Laurent *et al*, 1991; Hirschhorn *et al*, 1992; Peterson & Herskowitz, 1992). In mammalian cells, this multimeric protein complex is comprised of 10–15 subunits (Ho *et al*, 2009). Recent studies have revealed that there are three biochemically distinct mammalian SWI/SNF complexes—canonical BAF (cBAF), polybromo-BAF (PBAF), and non-canonical BAF (ncBAF), making SWI/SNF highly heterogeneous (Mashtalir *et al*, 2018). These complex subtypes share a common core made up of SMARCC1/2, SMARCE1, and SMARCD1/2/3 subunits (Mashtalir *et al*, 2018). SMARCA2 and SMARCA4 are the mutually exclusive, paralogous, catalytic ATPase subunits of the complex (Raab *et al*, 2017). Other complex-specific subunits like ARID1A/B (cBAF), PBRM1 and ARID2 (PBAF), GLTSCR1, and BRD9 (ncBAF) are essential for the proper deposition of the complex onto the chromatin via a direct association with various transcription factors and/or identification of a combinatorial histone code (Chandler Ronald *et al*, 2013; Alver *et al*, 2017; Porter & Dykhuizen, 2017; Ahmed *et al*, 2022). Notably, the SWI/SNF complex is mutated in approximately 25% of human cancers and its subunits like SMARCB1 and ARID1A are proposed to be tumor suppressors (Roberts *et al*, 2002; Kadoch *et al*, 2013).

Here, we show that the paraspeckles interact with the SWI/SNF complex. Notably, the paraspeckles interact only with the cBAF-type SWI/SNF, and this interaction is mediated by the DNA-binding ARID1B subunit. Consistent with this, the depletion of ARID1B disrupts the association of the PSPs with the SWI/SNF complex components. Moreover, we found that the association with PSPs is ARID1B specific, revealing a non-redundant role of the ARID1 paralogs. This interaction is enabled due to the binding of NEAT1 with ARID1B and hence, the loss of NEAT1 disrupts SWI/SNF association with paraspeckles. Functionally, NEAT1 and ARID1B coregulate transcription of genes involved in the regulation of splicing as well as alternative splicing. Overall, our study uncovers an interplay between the chromatin remodeler SWI/SNF and paraspeckle components in regulating transcription and alternative splicing.

Results

Purification of the PSPs reveals novel potential interactors

Paraspeckles have been implicated in important cellular processes, however, a clear understanding of how they function is lacking. This lack of understanding arises partly because of our limited knowledge of what the paraspeckles interact with as a complex. Based on the limited studies aimed at biochemical identification of the protein interactions of paraspeckles, the RNA-binding proteins PSPC1, SFPQ, and NONO have been described as their bonafide components (Naganuma *et al*, 2012; Mannen *et al*, 2016; An *et al*, 2019). SFPQ and NONO have been shown to heterodimerize and are deemed essential for the formation of paraspeckles (Knott *et al*, 2016). Although PSPC1 is a non-essential component of the paraspeckles, it can interact with SFPQ as well as NONO (Sasaki *et al*, 2009). Hence, we decided to purify these three proteins and look for their common interactors to understand the interactome of the paraspeckles.

For this, Halo-FLAG-tagged PSPC1, SFPQ, and NONO proteins were affinity purified using Halo ligand-conjugated magnetic resin from HEK293FRT nuclear extracts. Elution of the proteins purified this way involves cleaving off the Halo tag with TEV protease. To visualize the purified proteins, silver staining was performed (Fig 1A). For protein identification, the purified complexes were subjected to multi-dimensional protein identification technology (MudPIT) mass spectrometry (Dataset EV1). Ingenuity pathway analysis (IPA) of the proteins that were copurified with each of the PSPs revealed that they are predominantly involved in RNA processing, consistent with the known role of PSPC1, SFPQ, and NONO in these pathways (Kaneko *et al*, 2007; Peng *et al*, 2002; Wang *et al*, 2017; Fig EV1A). Purification of Halo-tag from cells stably expressing pcDNA5-Halo vector was used as a mock control. Notably, a common set of 685 proteins (log fold change > 1, Z-score > 2 over mock) were identified in the purifications of the three baits (Fig 1B). Not surprisingly, the GO term analysis of these 685 common interactors showed enrichment in RNA processing and splicing-related pathways (Fig 1C). Consistent with previous reports, all three proteins were copurified with one another (Fig 1D) (Knott *et al*, 2016). Furthermore, numerous constituents of the paraspeckles that were previously reported, such as FUS, PABPC4/1, YBX3, and PTBP1, were also copurified (An *et al*, 2019) (Fig 1D). Other proteins that populated this list of common interactors include the HNRNPs, SRSFs, snRNPs, and RBMs which are known to bind RNA molecules and regulate their splicing (Fig 1D). Interestingly, a closer

Figure 1. Paraspeckle proteins interact with canonical BAF-type SWI/SNF complex.

- A Silver-stained gel image of the affinity-purified complexes of PSPC1, SFPQ, and NONO. The respective proteins are marked along with ActEV protease used for the elution of purified proteins.
- B Venn diagram showing the overlap between the proteins copurified in the mass spectrometry.
- C GO-term analysis of common 685 interacting proteins using ShinyGO (<http://bioinformatics.sdstate.edu/go/>) identified by MudPIT in the affinity purification of PSPC1, SFPQ, and NONO.
- D, E Heat map showing the enrichment (dNSAFavg*1000) of proteins normalized to the bait (PSPC1, SFPQ, and NONO) focusing on (D) RNA processing and (E) SWI/SNF complex subunits.
- F Western blotting of affinity-purified complexes of PSPC1, SFPQ, and NONO with SWI/SNF antibodies. cBAF-, PBAF-, and ncBAF-specific, as well as common, subunits are marked.

Source data are available online for this figure.

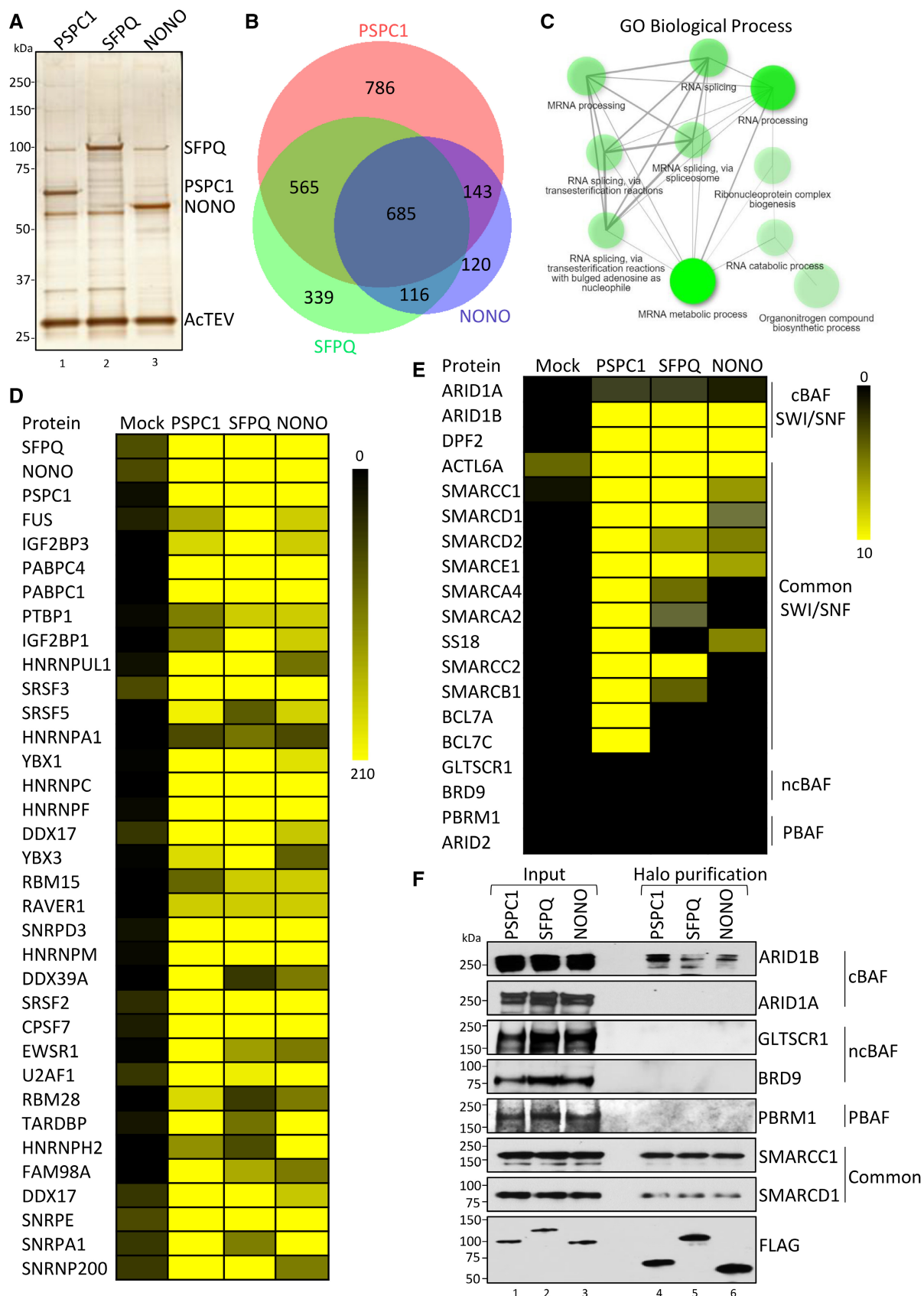


Figure 1.

inspection of the proteins that copurified with the bonafide PSPs revealed numerous transcription and chromatin-associated proteins including the mediator complex subunits, histones, DNA repair factors, proteasome subunits, as well as various SWI/SNF complex subunits (Fig 1E and Dataset EV1).

To conclude, the purifications of the PSPs—PSPC1, SFPQ and NONO—, in addition to validating some of the known interactions, revealed potential novel interactions of the paraspeckles. It has to be considered, although some of these interactions may not represent the interactome of the paraspeckle granules necessarily and might be exclusive to the PSPs.

Paraspeckle components interact with the cBAF-SWI/SNF complex

SWI/SNF has previously been found to colocalize with RNA-dependent bodies like nuclear stress bodies and paraspeckles (Kawaguchi & Hirose, 2015; Kawaguchi et al, 2015). However, the functional relevance of the possible paraspeckle-SWI/SNF interaction is not clear. Moreover, the subunit composition of the paraspeckle-localized SWI/SNF complex remains unknown. This becomes especially important to address as recent studies have revealed that there are at least three biochemically distinct mammalian SWI/SNF complexes—cBAF, PBAF, and ncBAF (Mashtalir et al, 2018). Hence, as both paraspeckles and SWI/SNF are multi-subunit entities, a comprehensive biochemical analysis is needed to better understand the significance of their possible interaction.

For this, we first wanted to understand which type of SWI/SNF complex associates with the paraspeckles. We found that many SWI/SNF subunits—including the core subunits—SMARCD1/2, SMARCC1, and SMARCE1, and the accessory component ACTL6A, were identified in all three purifications (Fig 1E). The ATPases—SMARCA2 and 4—, and other subunits, such as SMARCB1, SMARCC2, and BCL7A/C, were also detected in PSPC1 and SFPQ purifications. Notably, we found that the cBAF-specific subunits, ARID1B and DPF2, were copurified with all three PSPs that we purified (Fig 1E). Additionally, the lack of other SWI/SNF complex subtype-defining subunits like ARID2 and PBRM1 (of the PBAF complex) or GLTSCR1 and BRD9 (of the ncBAF complex) suggests that PSPs specifically interact with the cBAF-type SWI/SNF complex (Fig 1E).

Remarkably, ARID1B was markedly enriched over its paralog ARID1A in purifications of all three PSPs (Fig 1E). The MuDPIT results were validated by performing western blotting of the purified complexes with antibodies against the endogenous SWI/SNF subunits. As can be seen in the western blot data, ARID1B was detected in PSPC1, SFPQ, and NONO purifications unlike ARID1A (Fig 1F). Corroborating our mass spectrometry data, the SWI/SNF subunits—SMARCD1 and SMARCC1, which are essential for the formation of

the cBAF complex—, were also detected in all three purifications (Mashtalir et al, 2018) (Fig 1F). Furthermore, the PBRM1 component of PBAF type and BRD9 and GLTSCR1 subunits of ncBAF-type SWI/SNF complexes were not detected in these purifications (Fig 1F).

We, therefore, conclude that the PSPs copurify the cBAF-type SWI/SNF complex.

The PSPs preferentially interact with ARID1B over ARID1A

Our results suggest that not only PSPs interact with the cBAF SWI/SNF complex but surprisingly they also appear to prefer to bind ARID1B over ARID1A. This is interesting as, although ARID1A and 1B are paralogs, their non-redundant function has been proposed (Trizzino et al, 2018; Pagliaroli et al, 2021). Especially their opposing roles in regulating the cell cycle and distinct expression pattern has been previously described (Nagl et al, 2005; Flores-Alcantar et al, 2011). Hence, we wanted to confirm the association of paraspeckles with the ARID1B-SWI/SNF complex and explore the possible non-redundancy of the ARID1 paralogs.

To this end, we affinity-purified Halo-FLAG-tagged ARID1A and ARID1B from HEK293FRT nuclear extracts. The purified complexes were resolved on a 4–12% gradient gel, visualized by silver staining, and subjected to MuDPIT analysis (Fig 2A; Dataset EV2). Proteomic analysis revealed a significant enrichment (log-fold change > 2 and Z-score > 4 over mock) of 129 and 181 proteins with ARID1A and ARID1B, respectively. Purification of Halo-tag from cells stably expressing pcDNA5-Halo vector was used as a mock control. The GO term analysis of the top interactors (Z-score > 4) suggests that both the ARID1 paralogs are involved in chromatin-related processes and nucleosome disassembly, and are part of SWI/SNF complexes as expected (Fig 2B and C). Both the proteins also copurified various SWI/SNF subunits belonging to the cBAF complex (Fig 2C).

Strikingly, the IPA analysis of the top interactors of the ARID1 paralogs revealed a preferential association of ARID1B with RNA-splicing processes as compared to ARID1A (Fig 2B and D). Importantly, consistent with the purifications of PSPs, all three proteins—PSPC1, SFPQ, and NONO—were markedly enriched in ARID1B purifications as compared to that of ARID1A (Fig 2E). Further, we also found a greater enrichment of other PSPs including the HNRNPs, RBMs, DDX39A, CPSF7, PABPC1/4, PTBP1, and RAVR1 in the ARID1B purifications (Fig 2E). The interaction of the bonafide PSPs with ARID1B was further confirmed by performing western blotting of the purified complexes. Consistent with our MuDPIT data, PSPC1, SFPQ, and NONO were readily detected in ARID1B purification but not in ARID1A (Fig 2F). SMARCA4, the catalytic SWI/SNF subunit was copurified with both the ARID1 paralogs as expected.

Figure 2. ARID1B SWI/SNF complex interacts with various paraspeckle components.

- A Silver-stained gel image of the affinity-purified complexes of ARID1A and ARID1B. The bait and a few other SWI/SNF subunits are marked as per their molecular weight.
- B GO-term analysis (Biological Process) of the interacting proteins using ShinyGO identified by MudPIT in the affinity purification of ARID1A and ARID1B.
- C–E Heat maps showing the enriched proteins (dNSAFavg*1000) normalized to the bait identified in MudPIT analysis focusing on various (C) SWI/SNF subunits and (E) PSPs. (D) Graph showing the topmost processes picked up in the Ingenuity Pathway Analysis (IPA).
- F Western blotting of affinity-purified complexes of ARID1A and ARID1B with bonafide paraspeckle components. SMARCA4 was used as a positive control for purification.

Source data are available online for this figure.

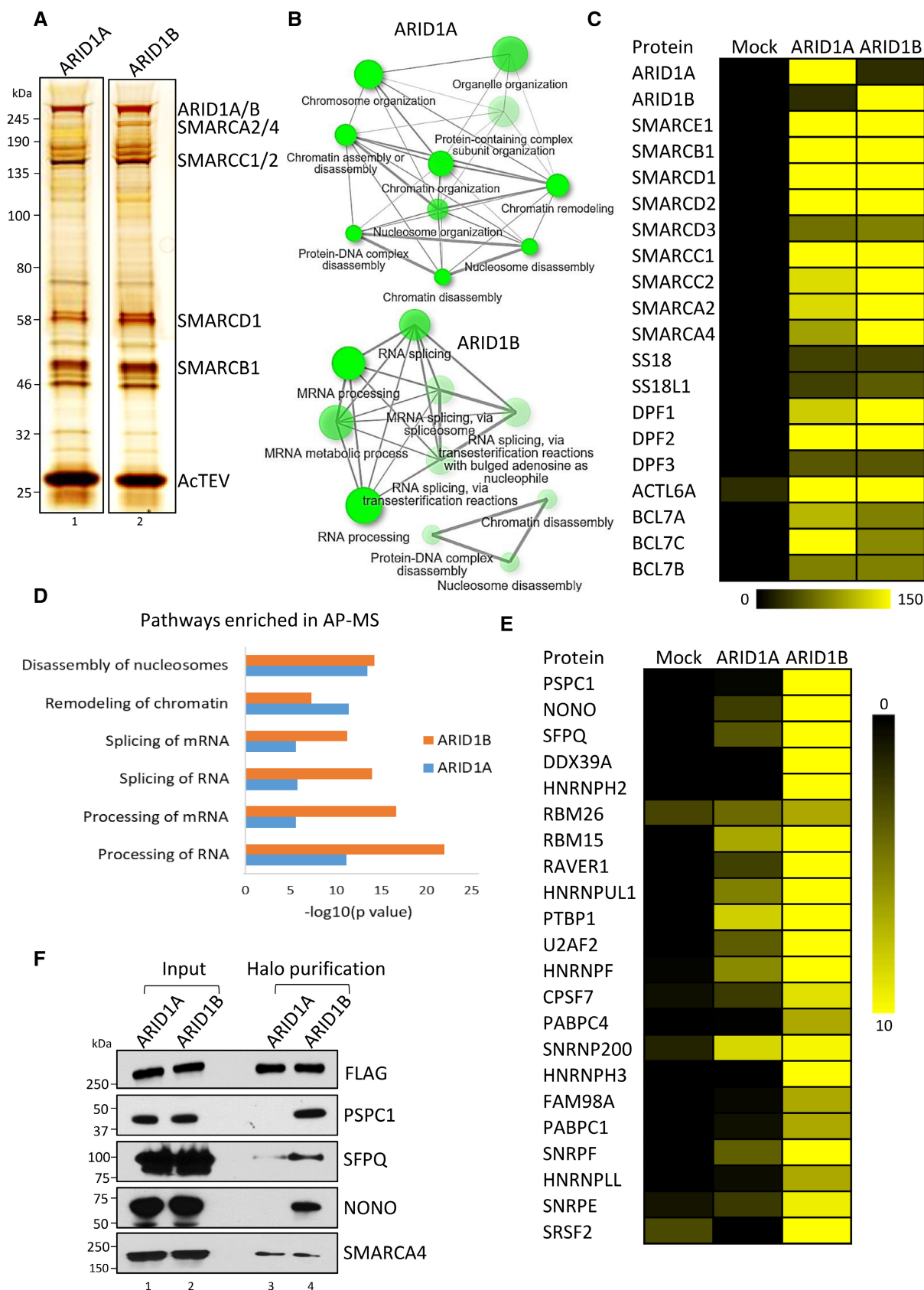


Figure 2.

For all the purifications performed thus far, we used the HEK293FRT cells. To test whether the ARID1B–PSP interaction also occurs in other cell types, Halo-FLAG-ARID1B was purified from the nuclear extracts of HeLa and HCT116 cells. Next, the purified ARID1B complexes were subjected to western blotting. Copurification of SMARCD1 was tested as a positive control for the purifications. Importantly, ARID1B copurified all three PSPs—PSPC1, SFPQ, and NONO—from these cell lines as well (Fig EV1B). The interaction was further confirmed by performing the reciprocal purification of Halo-FLAG-PSPC1 and testing its interaction with endogenous SWI/SNF subunits—ARID1B and SMARCD1—by western blotting (Fig EV1C).

Taken together, we conclude that the ARID1B-specific cBAF complex preferentially interacts with the PSPs.

The association of ARID1B SWI/SNF with the PSPs is NEAT1 dependent

To test whether the interaction of PSPs with ARID1B is affected by the presence of nucleic acids, we performed Halo purification of ARID1B in the absence and presence of a salt-active nuclease (SAN), which degrades both DNA and RNA. On performing western blotting of the purified complexes, it was observed that the interaction of ARID1B with PSPs—PSPC1, SFPQ, and NONO—persists (Fig EV1D). Considering that NEAT1 RNA is an integral component of the paraspeckles, we tested the status of NEAT1 in our nuclear lysates used for purification upon SAN treatment. For this, post-SAN treatment RNA isolation was performed from nuclear lysates. As expected, a marked reduction in the total nucleic acid content was observed upon loading equal volumes of SAN-treated and untreated lysates. Next, to check NEAT1 levels, cDNA synthesis was performed followed by PCR. Strikingly, the analysis suggests that NEAT1 levels remain unchanged upon SAN treatment, unlike GAPDH and 18 s rRNA (Fig EV1E). The distinct stability of NEAT1 upon nuclease treatment has been previously reported (An *et al*, 2019). NEAT1 is likely protected against nuclease treatment due to its interaction with numerous proteins within the paraspeckle granule.

To understand which paraspeckle component mediates the interaction with ARID1B cBAF, we first depleted PSPC1, SFPQ, NONO, and NEAT1 in 293FRT cells. The western blotting of input revealed that the siRNAs used were highly specific and resulted in the marked depletion of their target without much affecting the levels of other proteins of interest (Fig 3A). The pool of siRNA used for depleting NEAT1 targets both its isoforms and this was confirmed by qPCR as well as loss of NEAT1 signal in single-molecule FISH (smFISH; Fig EV2A and B).

Next, affinity purification of Halo-FLAG-ARID1B was performed and the purified complexes were subjected to western blotting to look for interaction with paraspeckle components (Fig 3A). Notably, only the depletion of NEAT1 resulted in the loss of interaction of ARID1B with all three PSPs—PSPC1, SFPQ, and NONO (Fig 3A). This suggests that the PSPs interact with ARID1B only in the presence of NEAT1.

To test the possibility that NEAT1 depletion might affect the SWI/SNF complex, first, the expression of various SWI/SNF subunits was tested upon NEAT1 depletion by western blotting (Fig EV2C). No striking changes were observed. ARID1B has previously been shown to associate with the SWI/SNF core by direct interaction with SMARCD1 (Mashtalir *et al*, 2018). Notably, there was no change in the interaction between ARID1B and SMARCD1 as well as with the ATPase subunit—SMARCA4—, upon depletion of PSPs or NEAT1, suggesting that they are not required for the incorporation of ARID1B into the SWI/SNF complex (Fig 3A).

NEAT1_2 has been shown as an essential component required for paraspeckle integrity and its depletion also leads to the loss of PSP–ARID1B interaction, emphasizing its role in governing paraspeckle–protein interactions. Hence, we wanted to understand in more detail how the loss of paraspeckle integrity changes the interactome of the PSPs. For this, Halo affinity purification of PSPC1, SFPQ, and NONO was performed from NEAT1-depleted 293FRT nuclear extracts. Silver-staining analysis of the purified complexes suggests that NEAT1 depletion does not have a prominent effect on the interaction of PSPC1, SFPQ, and NONO with one another (Fig EV2D). This was confirmed upon performing MudPIT analysis where the data showed that these three proteins continue to be the most abundant in each other's purification despite NEAT1's absence (Fig 3B; Dataset EV3). This is interesting as it suggests that the bonafide PSPs can continue to interact with one another without being part of the paraspeckles. However, of the 685 proteins that we found to interact with the three PSPs, almost half of the proteins (338) lost interaction upon NEAT1 depletion (Fig EV2E). This includes the RNA-binding proteins such as FAM98A, CPSF7, and FUS which have been previously shown to be part of paraspeckles (Fig 3B). Not surprisingly, the GO-term analysis of the proteins that lose interaction with the PSPs upon NEAT1 depletion revealed that they are enriched in pathways belonging to RNA processing (Fig 3C). These proteins among others likely require NEAT1 to assemble with the complex of PSPC1, SFPQ, and NONO to form the paraspeckle granules.

Importantly, corroborating our earlier results, the proteins that lost interaction with the three PSPs upon NEAT1 depletion include ARID1B (Fig 3D). Further, the interaction of the PSPs with other SWI/SNF subunits, including the core subunits (SMARCD1 and 2),

Figure 3. SWI/SNF interacts with PSPs in a NEAT1-dependent manner.

- A Halo purification was performed from nuclear extracts of scramble and various knockdown HEK293FRT cells expressing Halo-FLAG-tagged ARID1B. Input and eluted samples were resolved on a gel followed by western blotting with various antibodies. Western with SWI/SNF subunits—SMARCA4 and SMARCD1—were used as the control for purification, while beta-actin was used as a loading control.
- B–D (B) Heat map of the dNSAF (*1000) values of PSPs and (D) various SWI/SNF subunits in control (C) and NEAT1-depleted (KD) cells for PSPC1, SFPQ, and NONO purification from MudPIT analysis. (C) GO-term analysis was performed for interactions lost post-depletion of NEAT1.
- E, F (E) RIP qPCR and (F) PCR analysis was performed for monitoring NEAT1_2 levels, using an antibody against endogenous ARID1B. RIP with NONO and IgG was used as a positive and negative control, respectively. GAPDH levels were also assessed in the assay. Data are expressed as a percent of input. Error bars represent the standard error of three technical repeats (two-tailed *t*-test *****P* < 0.0001).

Source data are available online for this figure.

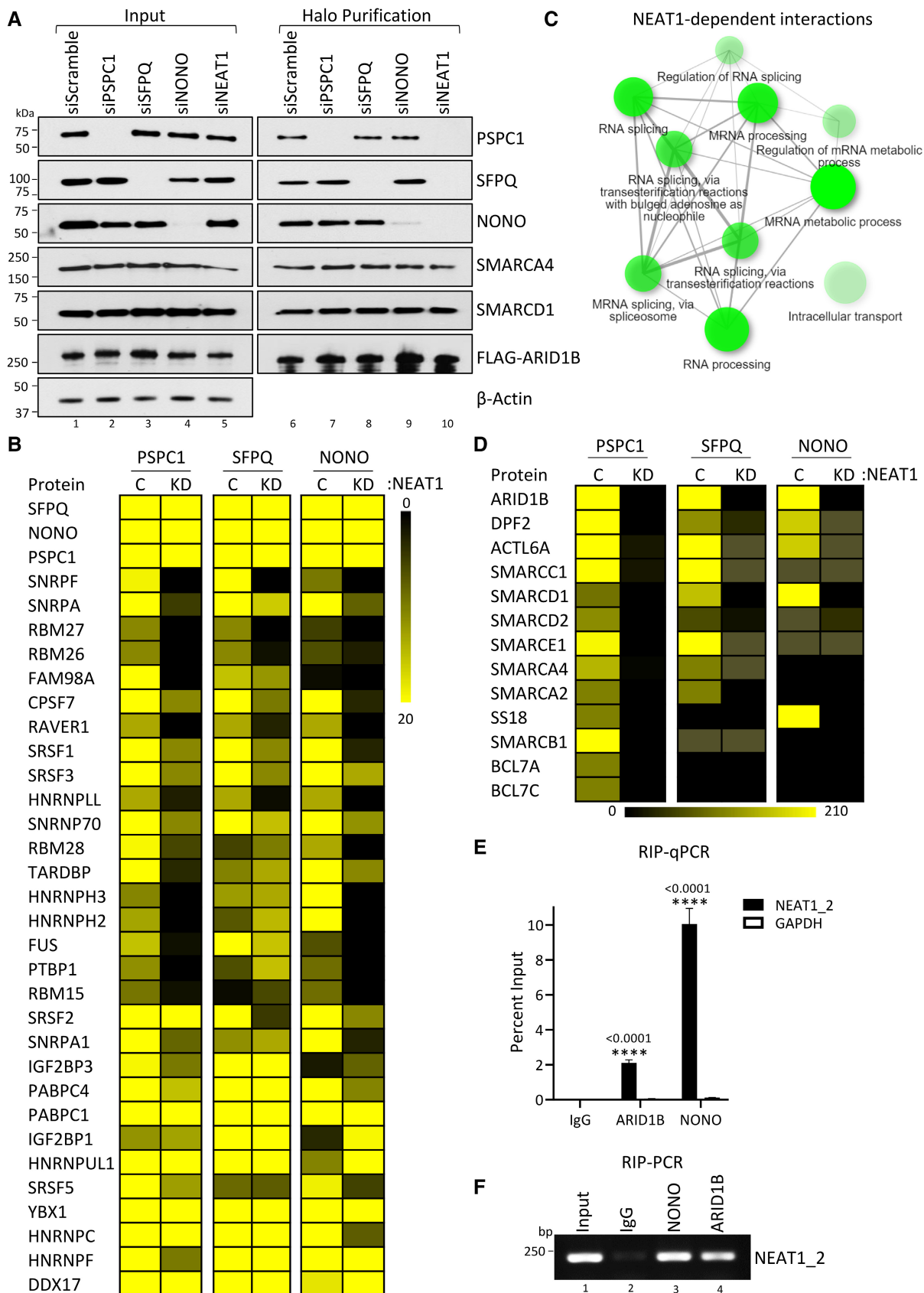


Figure 3.

ATPase subunits (SMARCA2 and 4), and cBAF-specific component (DPF2), was markedly reduced upon NEAT1 depletion (Fig 3D). This suggests that NEAT1 mediates the interaction of PSPs with the ARID1B–cBAF complex.

Next, we investigated whether ARID1B directly associates with NEAT1_2. To this end, we performed an RNA immunoprecipitation (RIP) assay using an antibody against endogenous ARID1B. The RNA thus obtained was subjected to cDNA synthesis and qPCR was performed. RIP with NONO was used as a positive control as it is known to directly bind NEAT1_2. Notably, NEAT1_2 was detected in RIP of both ARID1B and NONO by both qPCR and PCR analyses (Fig 3E and F). Further, the specificity of the RIP assay was confirmed by the lack of binding to a random, yet abundant transcript GAPDH (Fig 3E). We, therefore, conclude that ARID1B binds NEAT1_2.

ARID1B mediates the interaction of the cBAF-SWI/SNF complex with the PSPs

We found that the association of ARID1B–cBAF SWI/SNF complex with the PSPs is NEAT1 dependent. Our data also suggest that this is specific to the ARID1B protein. To test whether the interaction of PSPs and the SWI/SNF complex is mediated by ARID1B, we first generated stable ARID1B knockdown in HEK293FRT cells. Western blotting of the whole-cell lysates confirmed the specific depletion of ARID1B without affecting the expression of ARID1A (Fig EV2F). Next, we expressed and purified Halo-FLAG-SFPQ and Halo-FLAG-NONO from ARID1B-depleted cells. Silver-stained gel analysis of the purified complexes suggested that SFPQ and NONO were still copurified with one another (Fig EV2G). The band corresponding to PSPC1 could also be seen (Fig EV2G). This was further confirmed by MuDPIT analysis of the purified complexes (Dataset EV4). Remarkably, the depletion of ARID1B resulted in the loss of interaction of PSPs with other SWI/SNF subunits (Fig 4A). Notably, the non-existence of ARID1A in PSP purifications upon depletion of ARID1B indicates the non-redundancy between the ARID1 paralogs in mediating PSPs–SWI/SNF interaction (Fig 4A).

Interaction with ARID1B cBAF enables paraspeckles to engage chromatin-associated proteins

The loss of PSPs–SWI/SNF interaction upon ARID1B depletion prompted us to check whether this also affects paraspeckle formation. For this, we analyzed our MuDPIT data to look for changes in the interaction between the paraspeckle proteins. The interaction of the various NEAT1-dependent PSPs with SFPQ and NONO that we identified earlier did not show a significant change upon ARID1B depletion, suggesting that ARID1B is not essential for paraspeckle formation (Fig 4B). To further validate this, paraspeckles were visualized under the microscope by performing NEAT1 SmFISH. Consistent with our proteomics data, ARID1B depletion did not have a

noticeable effect on the number of paraspeckle puncta (Fig 4C). In comparison, the depletion of NONO, which is known to be important for paraspeckle formation, resulted in a significant reduction in the number of paraspeckle puncta as expected (Fig 4C).

ARID1B depletion did not result in a change in the association of PSPs with one another (Fig 4B). However, our proteomics data revealed that in addition to losing interaction with the SWI/SNF complex, ARID1B depletion also results in the loss of interaction of SFPQ and NONO with numerous transcription and chromatin-associated proteins (Fig 4D). This includes chromatin-modifying enzymes like JMJD6 and KMT2B; histone chaperones—ANP32B and NPM1; transcription factors—EP400, ERCC2, ATXN2L, and CTCF; the mediator complex subunits; and histones (Fig 4D). Notably, a few of these proteins were also copurified with ARID1B (Dataset EV2). This suggests that the interaction with ARID1B not only enables PSPs to interact with the SWI/SNF complex but also may provide them with means to gain access to the chromatin proteins including transcription factors.

ARID1A and 1B have non-redundant outcomes on the transcriptome

The biochemical characterization performed by us revealed interesting findings regarding the interaction between PSPs and the SWI/SNF complex and the importance of NEAT1 and ARID1B in mediating these interactions. Next, we wanted to understand the functional consequence of these associations. First, we wanted to focus on the ARID1 paralogs.

ARID1A and ARID1B are the mutually exclusive paralogous subunits of the cBAF complex (Raab *et al*, 2015). Both have the DNA-binding ARID domain and are often considered functionally interchangeable (Wang *et al*, 2004). We found that the PSPs preferentially bind to ARID1B over ARID1A. Moreover, we found that even in the absence of ARID1B, ARID1A does not mediate the interaction between SWI/SNF and PSPs. These observations support the possibility of non-redundant roles for the ARID1 paralogs.

To explore this idea further, RNA-seq was performed post-specific depletion of ARID1A and ARID1B in HEK293FRT cells to look for changes in the transcriptome. The depletion of the target transcripts was first validated using gene-specific primers (Fig 5A). Importantly, ARID1A depletion did not significantly alter the transcript level of ARID1B and vice versa (Fig 5A). We observed a similar specificity of depletion in our RNA-seq datasets as well (Fig EV3A). The data from these knockdowns revealed a global perturbation in transcription upon ARID1A and ARID1B depletion (Fig 5B). The depletion of ARID1A led to 853 up- and 137 downregulated (FDR < 0.05, fold change > 2) genes, while ARID1B knockdown had a more pronounced effect on the transcriptome with 1,263 up- and 230 downregulated genes (Fig EV3B and C;

Figure 4. ARID1B subunit mediates the interaction of paraspeckles with SWI/SNF and numerous chromatin-associated proteins.

- A, B, D Heat map showing the enrichment of (A) SWI/SNF subunits, (B) PSPs, and (D) chromatin-associated proteins in MudPIT analysis. C is control and KD is ARID1B-depleted cells.
- C smFISH analysis was performed to detect NEAT1 signal in the nucleus. The scale bar corresponds to 10 μ m. Graph showing the FISH signal quantification across the knockdowns in comparison to scramble control. The number of nuclei (*n*) used for quantification is mentioned. The error bars represent the standard error of three biological experiments (two-tailed *t*-test *******P* < 0.0043, ns > 0.05)

Source data are available online for this figure.

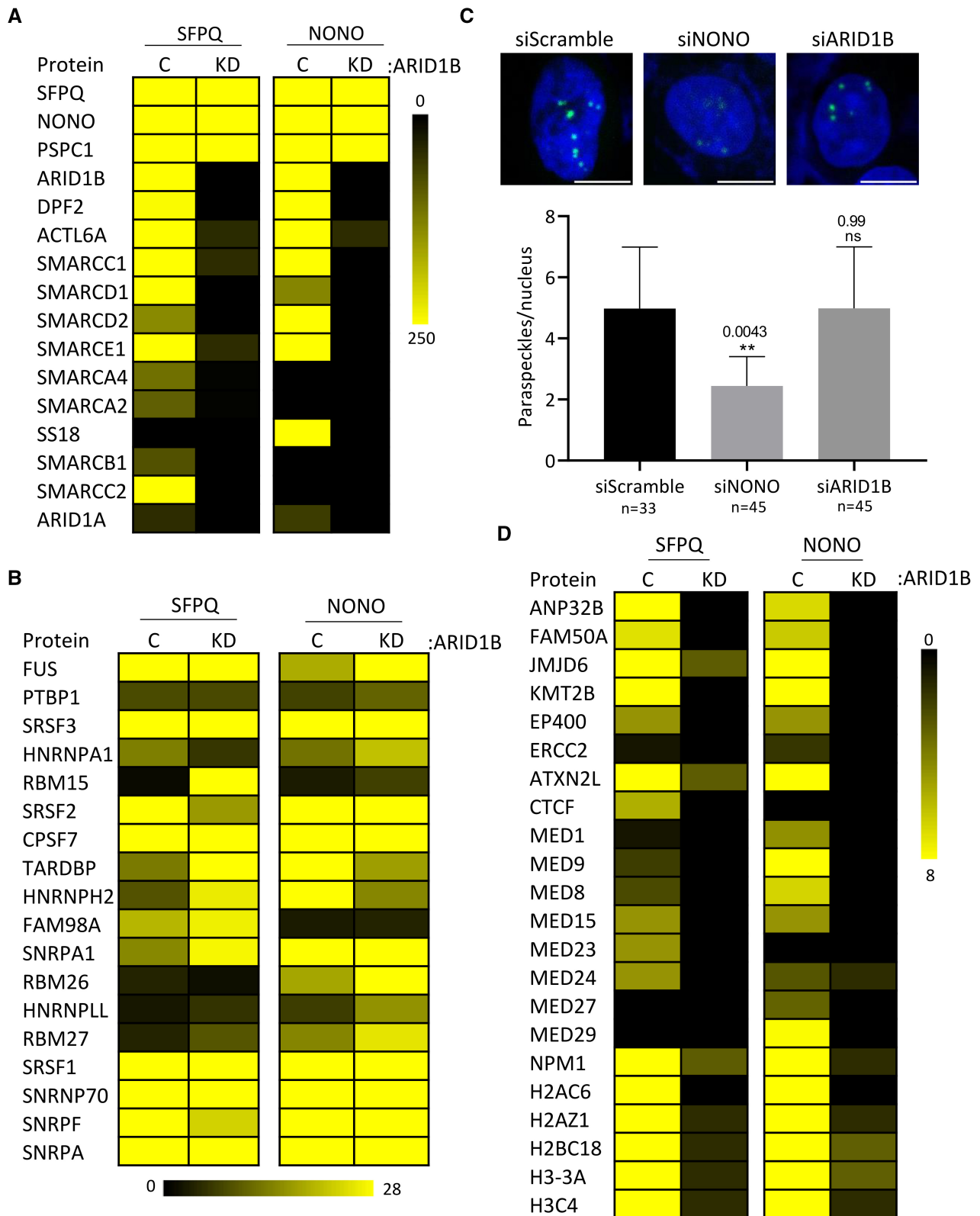


Figure 4.

Dataset EV5). Interestingly, a significant fraction of the genes regulated by ARID1A and ARID1B were non-overlapping suggesting a non-redundancy (Figs 5C and D, and EV5D). As the SWI/SNF

complex is generally associated with transcriptional coactivation, we next focused on the downregulated genes. The GO term analysis of the unique 184 downregulated genes revealed that ARID1B

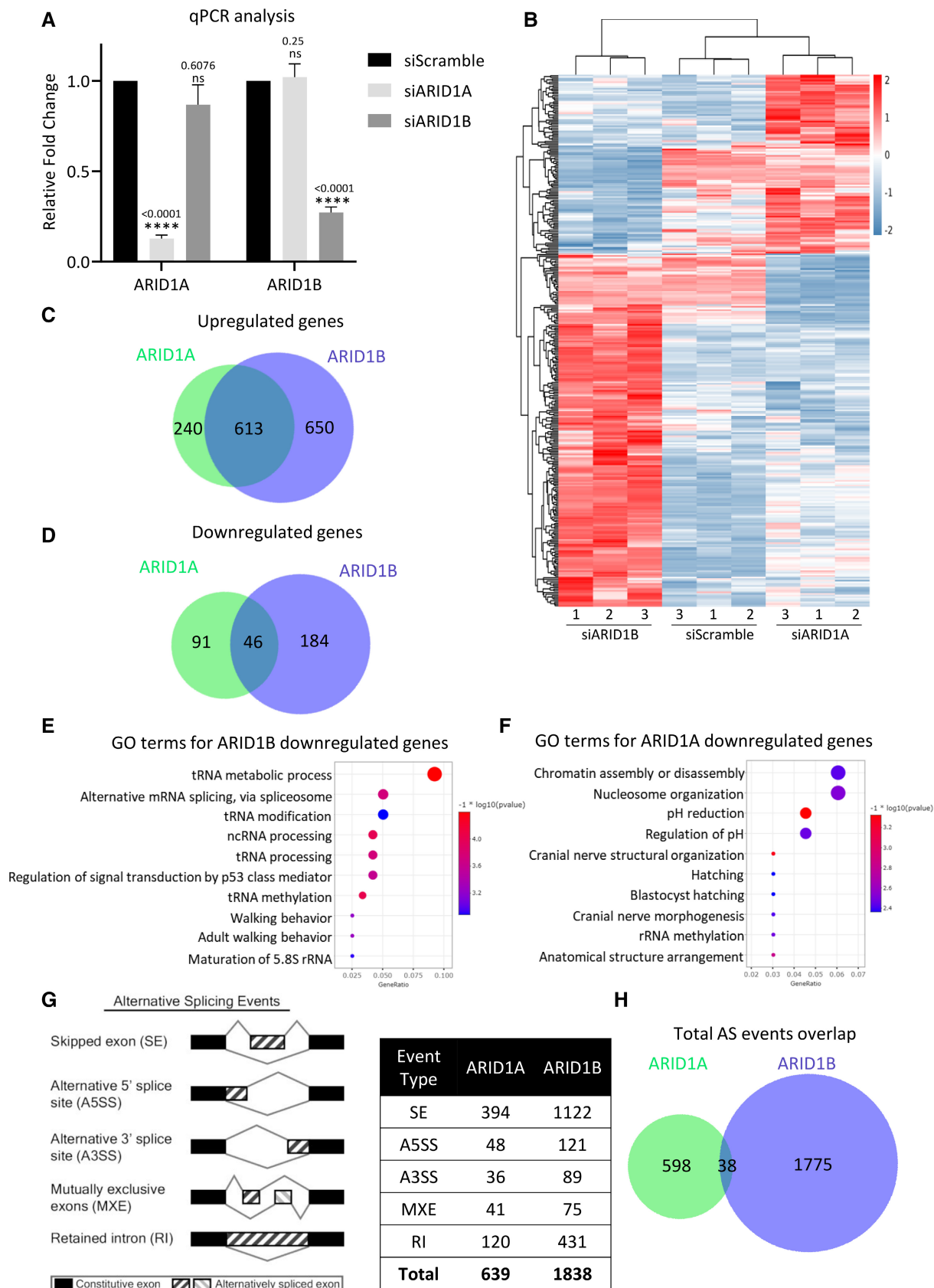


Figure 5.

Figure 5. ARID1 paralogs govern expression and AS of non-overlapping sets of genes.

- A RNA was isolated from HEK293FRT cells transfected with scrambled, ARID1A, or ARID1B siRNA, and qPCR was performed to check transcript levels. Values were normalized to GAPDH expression. Error bars represent the standard error of three different biological experiments performed in biological triplicates (two-tailed t-test **** $P < 0.0001$, ns > 0.05).
- B Heat map showing the widespread expression changes upon depletion of ARID1A or ARID1B.
- C, D Venn diagrams show the overlap of up- and downregulated genes upon ARID1A and ARID1B depletion as compared to scramble siRNA-treated cells.
- E, F Pathway analysis was performed for the specific genes downregulated upon ARID1B or ARID1A depletion.
- G Table showing the number of alternative splicing defects observed upon depletion of either ARID1A or ARID1B.
- H Venn diagram depicting the overlap between various splicing events in ARID1A and ARID1B.

regulates processes involved in the RNA, ncRNA, and tRNA processing pathways (Fig 5E). This was not observed for ARID1A-specific genes (Fig 5F).

Next, the RNA-Seq data were analyzed using the rMATS algorithm to look for alternative splicing (AS) changes. Changes in 639 and 1838 (FDR < 0.001) AS events were identified upon the depletion of ARID1A and ARID1B, respectively, as compared to the scramble siRNA-treated cells (Fig 5G; Dataset EV6). Different types of AS changes were observed with skipped exon (SE) events being the most affected. Notably, ARID1B depletion resulted in a markedly higher number of AS aberrations as compared to ARID1A and is consistent with our proteomic analysis which revealed enrichment of RNA-processing proteins in ARID1B purification (Fig 2). Further, the AS events were highly specific for ARID1A and ARID1B as irrespective of the type of AS event affected, only a meager overlap between them was observed (Figs 5H and EV5E).

Taken together, ARID1B not only interacts with PSPs but is also predominantly involved in the regulation of transcription and AS of various splicing-associated genes.

NEAT1 and ARID1B coregulate RNA-processing pathways

Paraspeckles are enriched in proteins such as the HNRNPs, SRSFs, and RBMs that are involved in RNA processing. Moreover, NEAT1 depletion not only leads to the loss of interaction of ARID1B with PSPs but it also has been linked with the regulation of the splicing of various genes involved in neuronal homeostasis in mice (Kukharsky et al, 2020). Considering that these two multi-subunit entities associate with one another, it is reasonable to speculate that they might regulate a common subset of genes.

To test this, a high-throughput RNA-seq analysis was performed post-depletion of the essential architectural component of the paraspeckles, NEAT1. NEAT1 depletion caused a global

perturbation in transcription, with 1,135 up- and 1,040 downregulated genes (FDR < 0.05 , fold change > 1.5) (Fig 6A). Notably, the transcription of 327 genes that were differentially expressed upon ARID1B knockdown also showed significant changes upon the depletion of NEAT1 (Fig EV4A). Interestingly, the GO-term analysis of the commonly downregulated genes revealed that they are enriched in pathways corresponding to ncRNA, rRNA, and other RNA-processing pathways (Fig 6B).

Next, we performed rMATS analysis to look for AS changes. This revealed that NEAT1 depletion affected a total of 3,053 splicing events (Fig 6C). We then categorized all the AS events obtained as up- or downregulated using the positive and negative inclusion difference values obtained by performing the rMATS analysis (Dataset EV5). This revealed that the majority of the altered AS events (69%) are downregulated upon NEAT1 depletion in comparison to scramble siRNA treatment (Fig 6D).

Next, we followed a similar template of analysis as previously published to understand the overlap between ARID1B and NEAT1 depletion (Huang et al, 2012; Bhattacharya et al, 2021a, 2021b). For this, using the inclusion-level parameters, we looked for an overlap between the individual up- and downregulated events (Fig EV4B). Strikingly, 70% of the overlapping events regulated by ARID1B and NEAT1 occur in the same direction (62% up- and 8% downregulated) (Fig 6E). This type of change in AS was prominent, especially for overlapping A5SS and RI types of events (Fig 6E). Further, a GO-term analysis of the total overlapping AS events revealed enrichment in pathways corresponding to RNA splicing (Fig EV4C). These AS changes can be visualized by looking at the genome browser tracks of genes such as PRPF39 and METTL17 for RI, and RBM5 and PRRC2C showing SE-type splicing events (Fig 6F, H, J, and L). Depletion of either NEAT1 or ARID1B led to the retention of intron 3 for PRPF39 and intron 9 for METTL17. It also affects the inclusion of exon 12 for RBM5 and exon 13 for PRRC2C.

Figure 6. NEAT1 and ARID1B coregulate AS.

- A Volcano plot showing the widespread gene expression changes observed upon knockdown of NEAT1 along with specific numbers.
- B Pathway analysis pertaining to biological function for the overlapping set of downregulated genes for NEAT1 and ARID1B.
- C Tabulated number of the alternative splicing events observed upon NEAT1 depletion in comparison with scramble-treated sample with a conservative FDR < 0.001 .
- D Pie chart showing the overall direction NEAT1-regulated splicing changes with percentage. The chart was plotted using the inclusion-level values obtained after rMATS analysis.
- E Pie charts depicting the direction of overlapping NEAT1 and ARID1B coregulated total, RI, and A5SS-type AS events. UP and DOWN represent the increase or decrease in AS events, respectively, based on the inclusion-level changes of exons or intron based on rMATS analysis.
- F–M Genome browser view showing (F, H) retention of introns 3 and 9 for PRPF39 and METTL17 (J, L) inclusion of exons 12 and 13 for RBM5 and PRRC2C, respectively, upon NEAT1 and ARID1B depletion in comparison to scramble-treated control. Exon and intron numbers are marked. (G, I, K, M) PCR validation of the AS changes seen upon knockdown of NEAT1 and ARID1B in comparison to scramble. For PRPF39, primer pair was designed against exons 3 and 4, encompassing intron 3 and for METTL17, primers against exons 9 and 10 were used. For SE-type AS changes, primers against exons 11, 13, 12, and 14 were for RBM5 and PRRC2C, respectively.

Source data are available online for this figure.

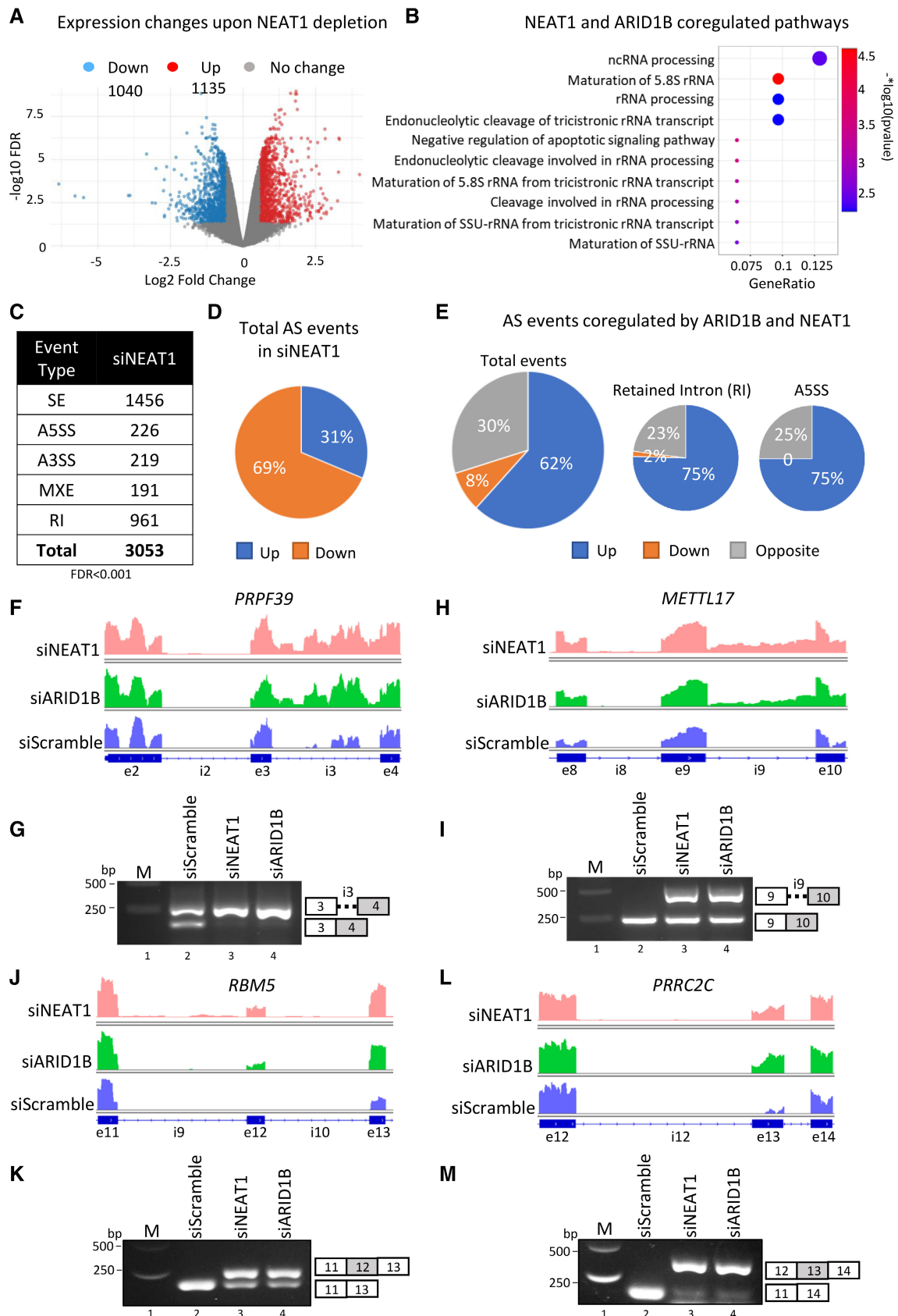


Figure 6.

Next, we validated a few of the AS changes observed in our RNA-seq analysis by performing PCR in an independent knockdown experiment by using specific primers encompassing the retained intron or skipped exon (Fig 6G, I, K, and M). Collectively, these results suggest that NEAT1 and ARID1B can regulate overlapping sets of transcription and AS events.

To understand if the transcriptomic changes mediated by the loss of ARID1B/NEAT1 are direct targets, ARID1B ChIP was done in replicate and this along with input was subjected to sequencing. A total of 1,451 ARID1B peaks corresponding to 1,381 genes were identified using macs2 with a *q*-value of 0.05. Annotation of these peaks and genome distribution analysis suggest that around 30% of the peaks occupy intronic regions (Fig EV5A). This unique genomic distribution of ARID1B has been previously reported (Raab et al, 2015). Next, the GO-term analysis of the ARID1B-occupied genes (1381) suggests they correspond to pathways related to transcription, in agreement with the known role of ARID1B-SWI/SNF as a transcription coactivator (Fig EV5B). Notably, pathways related to RNA biosynthesis and metabolism were also enriched (Fig EV5B). Next, we could detect the overlap of 38 genes between AS changes coregulated by ARID1B/NEAT1 and the ARID1B ChIP genes (Fig EV5C). Further, GO-term analysis of the 38 genes reveals they pertain to pathways corresponding to RNA processing and splicing (Fig EV5D). The limited overlap obtained suggests that probably, ARID1B/NEAT1 largely regulates AS indirectly via regulating the expression/splicing of various genes involved directly in splicing. This is in corroboration with the GO analysis of the AS genes post-ARID1B/NEAT1 depletion which corresponds predominantly to splicing pathways (Fig EV4C).

Collectively, these results suggest that NEAT1 and ARID1B can regulate not only the transcription but also AS of genes associated with splicing.

Discussion

Two primary mechanisms have been proposed to explain how paraspeckles can influence cellular functions: (i) they can act as a molecular sponge to limit the interaction of various PSPs with their respective targets (Macias et al, 2012; Hirose et al, 2014) and (ii) trap mRNA and inhibit downstream processes such as nuclear export and translation (Prasanth et al, 2005). However, recent evidence suggests that binding with paraspeckles enables proper targeting of proteins like SRSF2 to certain genomic loci to bring about gene expression changes (Li & Wang, 2021). Further, NEAT1 also binds to chromatin and this is receptive to the transcriptional status of its genomic targets (West et al, 2014). Additionally, NEAT1 has also been shown to associate with numerous transcription repressors and coactivators like EZH2, CARM1, ASXL1, and ISWI, including SWI/SNF complexes (Kawaguchi et al, 2015; Hupalowska et al, 2018; An et al, 2019; Wang et al, 2019; Yamamoto et al, 2021). In agreement with these reports, we show that the loss of interaction with ARID1B-SWI/SNF led to reduced interaction of PSPs with various chromatin and transcription factors. Together, this evidence presents a third possible mechanism of functioning of paraspeckles, where paraspeckles can impart their effect by associating with chromatin. Maybe NEAT1 acts like a cargo carrier to which various RNA-processing factors bind

resulting in their enrichment. This arrangement likely acts as a hub to influence the synthesis or processing of the emerging RNA from large chromatin domains in its proximity and also enables the paraspeckles to dynamically respond to various external signals. The association with chromatin-remodeling complexes like SWI/SNF might be required for their specific targeting near gene loci and transcripts (Fig 7). Interestingly, the SWI/SNF-dependent regulatory activity of paraspeckles largely regulates AS of genes involved directly in splicing. Further, recent hybridization-based studies performed to understand the direct targets of NEAT1 using rat pituitary cells have shown that it can bind directly to the targets involved in RNA splicing (Torres et al, 2016; Jacq et al, 2021). However, the limited overlap between NEAT1 and ARID1B coregulated events also suggests that depending on the gene and the context, NEAT1 may probably rely on other transcription and epigenetic regulators for their targeting. This might also explain the previously observed DNA and RNA sequence-independent NEAT1 interaction (West et al, 2014; Torres et al, 2016; Jacq et al, 2021). One such protein which has been previously reported and observed in our study is SMARCA5, an ISWI chromatin remodeler (An et al, 2019).

The biochemical heterogeneity of the SWI/SNF complex can provide specific functions to the complex, which might result in greater regulatory control over transcriptional networks. Accordingly, cBAF, PBAF, and ncBAF complexes have been shown to colocalize with distinct transcription factors, at different genomic locations in various cellular contexts (Michel et al, 2018). cBAF is the most abundant complex and has been shown to perform a wide variety of functions attributed to the SWI/SNF complexes (Michel et al, 2018). The function of the other two complexes is relatively not well studied, but PBAF has been shown to maintain genome integrity during mitosis while ncBAF is essential during immune cell development (Brownlee et al, 2014; Loo et al, 2020). One interesting finding from our study is that the interaction with paraspeckles is specific to cBAF-type SWI/SNF complex. cBAF is the most abundant complex that is known to bind extensively at enhancers and promoters (Michel et al, 2018). This possibly makes it the best suited among the SWI/SNF complexes to bring paraspeckles near active chromatin sites. SWI/SNF subunits, especially SMARCA2, have been previously shown to regulate AS by modulating exon inclusion through transcription elongation rates and by direct interaction with the splicing factors such as Sam68 in mammalian cells (Batsché et al, 2006). A recent paper also noted that SMARCA4 binds to a greater proportion of primary transcripts as compared to well-known RNA-binding proteins (Raab et al, 2019). Further, BRM has also been shown to interact with pre-mRNPs in flies (Tyagi et al, 2009). All this evidence and our study suggest that SWI/SNF not only regulates the transcription of genes but also can influence their splicing outcome.

Strikingly, the interaction with paraspeckles is unique to the ARID1B subunit. ARID1A and 1B are often presumed to be redundant, and because of this, ARID1B has been proposed as a synthetic lethal target in ARID1A-mutated cancers (Helming et al, 2014). Contrary to this, evidence has emerged that suggests a non-redundant role of the ARID1A paralogs. Depletion of ARID1A leads to cell cycle arrest, unlike ARID1B (Wang et al, 2004). Additionally, ARID1A has been shown to regulate Poll II pausing, which cannot be replaced by ARID1B for a subset of genes in ovarian cancer cells (Trizzino

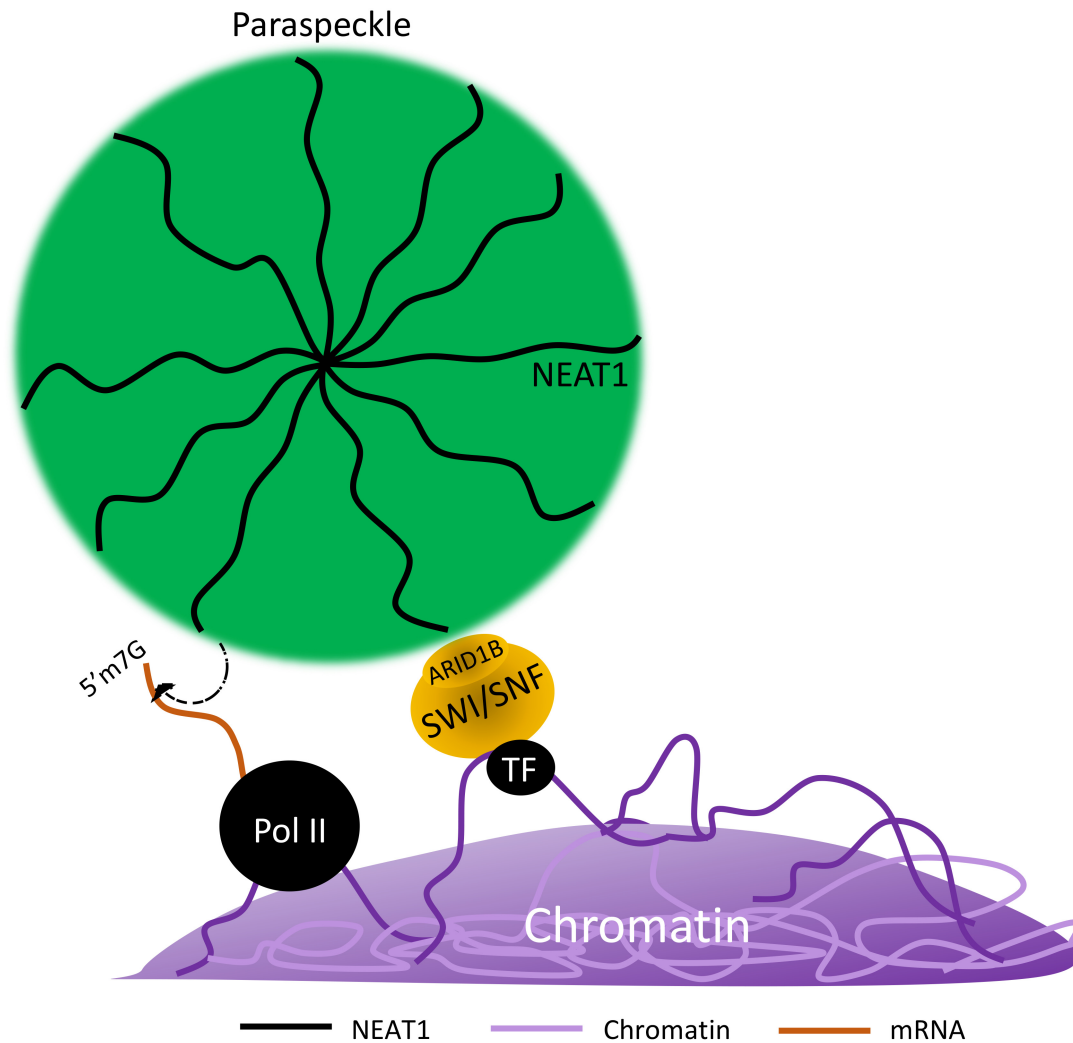


Figure 7. A hypothetical model showing the function of paraspeckle–SWI/SNF interaction.

An illustration speculating a possible mechanism of cross-talk between ARID1B cBAF-type SWI/SNF complex and paraspeckles. See text for details.

et al, 2018). Further, a global genomic analysis in HepG2 cells revealed that ARID1 paralogs may have antagonistic functions, with ARID1B acting as a repressor, as opposed to ARID1A, which mostly functions as an activator (Raab *et al*, 2015). Further, comparative genomic analysis has also shown that ARID1B uniquely associates with introns (Raab *et al*, 2015). More recently, ARID1B-containing cBAF has been shown to uniquely regulate neuroectoderm lineage specificity (Pagliaroli *et al*, 2021). Our findings not only add to the body of evidence that reveals a non-redundancy between the ARID1 paralogs but also reveals a greater insight into the basis of their non-redundancy. Notably, such functional specificity is not just restricted to the ARID1 paralogs. SMARCD2 has been shown to uniquely interact with the transcription factor, CEBPE, unlike its paralogs SMARCD1 and 3 to regulate granulocyte development (Priam *et al*, 2017). The molecular basis of the non-redundancy of SWI/SNF paralogs remains to be understood. It may arise due to the differences in interactions caused by variations in low-complexity sequences or intrinsically disordered regions, post-translational

modifications, stretches of charged or polar amino acid residues, etc. (Hennig *et al*, 2015; Strzyz, 2018). More than 75% of the sequence of ARID1 paralogs is predicted to be disordered and this might enable them to have specific interactions (El Hadidy & Uversky, 2019). However, more studies are needed to understand the basis of paralog specificities in detail.

It is noteworthy that mutations in ARID1B are associated with neurodevelopmental disorders and cancers like neuroblastoma (Sim *et al*, 2015). Accordingly, ARID1B-haploinsufficient mice display a wide variety of neuronal disarray, impaired social behavior, and growth (Celen *et al*, 2017; Jung *et al*, 2017). Interestingly, NEAT1 knockout mice also show a deficit in social interaction, and NEAT1 can regulate AS of genes involved in synaptic regulation (Kukharsky *et al*, 2020). The role of other PSPs in neuropathological conditions like Alzheimer's is also well recognized (Kamelgarn *et al*, 2018; Huang *et al*, 2020). It will be interesting to explore the possibility of ARID1B and NEAT1 in regulating neuronal development and disorders together in the future.

Materials and Methods

Plasmids

ARID1B human ORF was procured from Promega. ARID1A, PSPC1, SFPQ, and NONO plasmids were obtained from Addgene. All these were then subcloned into a pcDNA5FRT-Halo CMVD2 vector using AsiSI and PmeI enzymes. All constructs generated were confirmed by sequencing. ARID1A, ARID1B, NEAT1, and scramble-siRNA sequences were procured from Dharmacon. The catalog ID of the plasmids and siRNA sequences are provided in Table EV1.

Cell line maintenance and drug treatment

HEK293FRT cells were purchased from Invitrogen and maintained in DMEM with GlutaMAX and 10% FBS. Stable expression cell lines were generated using the Flp-In System (Invitrogen) according to the manufacturer's instructions. All stable expression cell lines used in this study were generated in HEK293FRT cells and maintained in DMEM with GlutaMAX, 10% FBS, and 100 µg/ml hygromycin B. For transient expression, FuGene6 (Promega) or polyethyleneimine, Linear, MW 25000 (polysciences), was used to transfect the expression vector into cells. All cells were maintained at 37°C in a 5% humidified incubator. Transfection of siRNAs was performed using Lipofectamine RNAi Max (Thermo Fisher) at 40% cell confluency.

Affinity purification

Stable cell lines were cultured in 150 mm dishes and expanded according to assay requirements and bait expression levels. Cells were scraped from plates and washed with cold PBS. The suspension was centrifuged at 3,000 rpm for 5 min at 4°C and pellets were resuspended in hypotonic buffer (10 mM Tris-HCl pH 7.5, 10 mM KCl, 1.5 mM MgCl₂, 1 mM DTT, and 1 mM PMSF) and incubated on ice for 5 min. The suspension was centrifuged at 5,000 rpm for 5 min at 4°C, and pellets were resuspended in five volumes of fresh HB-containing protease inhibitor cocktail and homogenized using a glass Dounce homogenizer. The suspension was layered onto an HB sucrose cushion containing 30% sucrose w/v, centrifuged at 5,000 rpm for 1 h at 4°C, and the cytosol-containing layer was discarded. The nuclei were lysed by resuspending in lysis buffer (50 mM Tris, pH 7.5, 150 mM NaCl, 1% Triton X-100, 0.1% N-dodecylcholate, and a protease inhibitor cocktail) and incubated on a rocker for 20 min at 4°C. The lysed cells were centrifuged at 16,000 g for 20 min. The supernatant was collected and diluted 1:3 by adding dilution buffer (1× PBS, pH 7.5 with 1 mM DTT, and 0.005% NP40). The diluted lysate was added to pre-equilibrated Magne® HaloTag® Beads (Promega, G7282) and incubated overnight on a rotator at 4°C. The beads were then washed with wash buffer (50 mM Tris-HCl, pH 7.5, 300 mM NaCl, 0.005% NP40, and 1 mM DTT). AcTEV (Thermo Fisher, 12575015) protease was used for elution.

Mass spectrometry analysis

Protein samples were analyzed by Multidimensional Protein Identification Technology (MudPIT), as described previously (Florens & Washburn, 2006). Briefly, precipitated proteins were resuspended in 30 µl of 100 mM Tris pH 8.5 with 8 M urea to denature proteins.

Cysteines were reduced and alkylated before digestion with recombinant LysC and modified trypsin. Reactions were quenched by the addition of formic acid to the final concentration of 5%. After digestion, peptide samples were pressure loaded onto 100 µm fused silica microcapillary columns packed first with 9 cm of reverse-phase material, followed by 3 cm of 5 µm Strong Cation Exchange material, and followed by 1 cm of 5 µm C18 RP. The loaded microcapillary columns were placed in line with a 1260 Quaternary HPLC. The application of a 2.5 kV distal voltage electrosprayed the eluting peptides directly into LTQ linear ion-trap mass spectrometers equipped with a custom-made nano-LC electrospray ionization source. Full-MS spectra were recorded on the eluting peptides over a 400 to 1,600 m/z range, followed by fragmentation in the ion trap on the first- to fifth-most intense ions selected from the full-MS spectrum. Dynamic exclusion was enabled for 120 s (Zhang et al, 2009). Mass spectrometer scan functions and HPLC solvent gradients were controlled by the XCalibur data system.

RAW files were extracted into .ms2 file format using RawDistiller v. 1.0, in-house developed software (McDonald et al, 2004; Zhang et al, 2011). RawDistiller D(g, 6) settings were used to abstract MS1 scan profiles by Gaussian fitting and to implement dynamic offline lock mass using six background polydimethylcyclsiloxane ions as internal calibrants. MS/MS spectra were first searched using ProLuCID with a mass tolerance of 500 ppm for peptide and fragment ions (Xu et al, 2015). Trypsin specificity was imposed on both ends of candidate peptides during the search against a protein database containing 44,080 human proteins (NCBI 2019-11-03 release), as well as 426 common contaminants such as human keratins, IgGs, and proteolytic enzymes. To estimate false discovery rates (FDR), each protein sequence was randomized (keeping the same amino acid composition and length) and the resulting "shuffled" sequences were added to the database, for a total search space of 89,038 amino acid sequences. Masses of 57 Da were differentially added to cysteine residues to account for alkylation by CAM and that of 16 Da were differentially added to methionine residues.

DTASelect v.1.9 was used to select and sort peptide/spectrum matches (PSMs) passing the following criteria set: PSMs were only retained if they had a ΔCn of at least 0.08; minimum XCorr values of 1.8 for singly-, 2.1 for doubly-, and 2.5 for triply-charged spectra; peptides had to be at least 7 amino acids long. Results from each sample were merged and compared using CONTRAST (Tabb et al, 2002). Combining all replicate runs, proteins had to be detected by at least two peptides and/or two spectral counts. Proteins that were subsets of others were removed using the parsimony option in DTASelect on the proteins detected after merging all runs. Proteins that were identified by the same set of peptides (including at least one peptide unique to such protein group to distinguish between isoforms) were grouped, and one accession number was arbitrarily considered representative of each protein group.

NSAF7 was used to create the final reports on all detected peptides and non-redundant proteins identified across the different runs (Zhang et al, 2010). Spectral and peptide-level FDRs were, on average, $0.52 \pm 0.41\%$ and $0.39 \pm 0.1\%$, respectively. QPROT was used to calculate a log-fold change and Z-score for the samples compared to the mock control (Choi et al, 2015). Purification of Halo from cells expressing empty Halo vector was used as a mock.

For instances where there was more than one replicate analyzed by MudPIT, proteins with log-fold change > 1 and Z-score > 2 or 4

were further analyzed in IPA (Qiagen) to determine pathways enriched by the bait proteins. For proteins with only one replicate, a ratio was calculated of dNSAF values between the sample and mock. For those to be further analyzed in IPA or Shiny GO, the dNSAF ratio had to be > 2 compared to mock. Pathways were considered significantly enriched with P -value < 0.05 ($-\log_{10}(P\text{-value}) > 1.3$).

Isolation of total RNA and PCR

Total RNA was extracted from cells as per the manufacturer's (Qiagen) instructions. It was further treated with DNaseI (NEB) for 30 min at 72°C to degrade any possible DNA contamination. RNA (2 μ g) was subjected to reverse transcription using QScript cDNA synthesis mix according to the manufacturer's instructions. cDNAs were then amplified with the corresponding gene-specific primer sets. For RT-PCR, PCR was conducted for 24 cycles using the condition of 30 s at 94°C, 30 s at 60°C, and 30 s at 72°C. The PCR products were analyzed on 1% agarose gels containing 0.5 μ g/ml ethidium bromide. The sequence of oligos used is provided in Table EV2.

Antibodies

ARID1A (CST D2A8U, dilution 1:2,000), ARID1B (Abcam ab57461, dilution 1:3,000) FLAG (Sigma-Aldrich A8592, dilution 1:10,000), Halo (Promega G9211, dilution 1:5,000), PSPC1 (Sigma, SAB4200503, 1: 5,000), SFPQ (Abcam, ab38148, 1:2,000), NONO (Santa Cruz, sc-166,702 X, 1:8,000), SMARCA4 (ab110641, Abcam, 1: 2,000), SMARCD1 (Santa Cruz, sc-135,843, 1:1,000), SMARCE1 (Bethyl laboratories, A300-810A, 1:5,000), SMARCB1 (Abcam, ab58209, 1:1,000), SMARCC1 (CST, 11956S, 1: 2,000), and β -actin (Abcam ab8224, dilution 1:2,500).

High-throughput sequencing

Sequencing libraries were prepared using High Throughput Library Prep Kit (KAPA Biosystems) following the manufacturer's instructions. The library was sequenced on an Illumina HiSeq platform with paired reads of 75 bp for RNA-seq.

RNA-seq analysis

Raw reads were demultiplexed into FASTQ format allowing up to one mismatch using Illumina bcl2fastq2 v2.18. Reads were aligned to the human genome (hg38 and Ensembl 96 gene models) using STAR (version STAR_2.6.1c). TPM expression values were generated using RSEM (version v1.3.0). edgeR (version 3.24.3 with R 3.5.2) was applied to perform differential expression analysis, using only protein-coding and lncRNA genes. To perform differential splicing analysis, we used rMATs (version 4.0.2) with default parameters (Shen *et al*, 2014). FDR cut-off of 0.001 was used to determine statistical significance.

smFISH

A commercially available NEAT1 probe (Stellaris FISH probe for human NEAT1, 5' segment; Biosearch Technologies) was used as per the manufacturer's protocol. Briefly, cells were fixed with 4%

PFA for 15 min, followed by permeabilization with 0.5% Triton X-100 for 5 min. Cells were incubated in 10% formamide/2 \times SSC for 10 min at RT followed by hybridization at 37°C for 16 h. Samples were mounted in ProLong Diamond antifade reagent (Thermo Fisher). Quantification was performed using ImageJ software (National Institutes of Health).

RIP assay

Cross-linking RIP assay was performed using Magna Nuclear RIP kit (Millipore) as per manufacturer's instructions using ARID1B and NONO antibody. Briefly, cells were cross-linked by 1% formaldehyde for 10 min and then quenched in 125 mM glycine for 5 min. After washing with cold 1 \times PBS thrice, cells were harvested by scraping and pelleted down by centrifugation. The nuclei isolated were then lysed in a complete RIP lysis buffer. A total of 100 μ l of the extract was incubated with RIP buffer containing protein G agarose beads conjugated with antibodies against ARID1B, NONO, or control IgG antibodies (Millipore) for 6 h at 4°C. The beads were washed with wash buffer, and then the complexes were incubated with 0.1% SDS/0.5 mg/ml proteinase K (30 min at 55°C) to remove the proteins. Finally, the immunoprecipitated RNA was purified and analyzed by qRT-PCR.

Data availability

The RNA seq datasets are available in the Gene Expression Omnibus (GEO) database under the accession number GSE199631 (<http://www.ncbi.nlm.nih.gov/geo/query/acc.cgi?acc=GSE199631>), while ChIP-seq data are under GSE214879 (<http://www.ncbi.nlm.nih.gov/geo/query/acc.cgi?acc=GSE214879>). The mass spectrometry proteomics data are available at the ProteomeXchange Consortium with the dataset identifier PXD032988 (<http://www.ebi.ac.uk/pride/archive/projects/PXD032988>) via the MassIVE repository and may be accessed at <ftp://msv000089198@massive.ucsd.edu>. Original data underlying this manuscript can be accessed from the Stowers Original Data Repository at <http://www.stowers.org/research/publications/libpb-1749>. Source data are provided with this paper.

Expanded View for this article is available [online](#).

Acknowledgements

This work was supported by funding from the National Institute of General Medical Sciences (grant no. R35GM118068) and the Stowers Institute for Medical Research to Jerry L Workman. The authors would like to thank the members of the Workman lab for their critical suggestions to improve the manuscript.

Author contributions

Divya Reddy: Conceptualization; data curation; formal analysis; validation; investigation; visualization; methodology; writing—original draft; writing—review and editing. **Saikat Bhattacharya:** Formal analysis; validation; methodology; writing—original draft; writing—review and editing. **Michaella Levy:** Software; methodology. **Ying Zhang:** Software; methodology. **Madelaine Gogol:** Software; methodology. **Hua li:** Software; methodology. **Laurence Florens:** Software; methodology. **Jerry L Workman:** Supervision; funding acquisition; project administration; writing—review and editing.

Disclosure and competing interests statement

The authors declare that they have no conflict of interest.

References

- Adriaens C, Standaert L, Barra J, Latil M, Verfaillie A, Kalev P, Boeckx B, Wijnhoven PW, Radaelli E, Vermi W et al (2016) p53 induces formation of NEAT1 lncRNA-containing paraspeckles that modulate replication stress response and chemosensitivity. *Nat Med* 22: 861–868
- Adriaens C, Rambow F, Bervoets G, Silla T, Mito M, Chiba T, Asahara H, Hirose T, Nakagawa S, Jensen TH et al (2019) The long noncoding RNA NEAT1_1 is seemingly dispensable for normal tissue homeostasis and cancer cell growth. *RNA* 25: 1681–1695
- Ahmed NS, Gatchalian J, Ho J, Burns MJ, Hah N, Wei Z, Downes M, Evans RM, Hargreaves DC (2022) BRD9 regulates interferon-stimulated genes during macrophage activation via cooperation with BET protein BRD4. *Proc Natl Acad Sci U S A* 119: e2110812119
- Alver BH, Kim KH, Lu P, Wang X, Manchester HE, Wang W, Haswell JR, Park PJ, Roberts CWM (2017) The SWI/SNF chromatin remodelling complex is required for maintenance of lineage specific enhancers. *Nat Commun* 8: 14648
- An H, Williams NG, Shelkovernikova TA (2018) NEAT1 and paraspeckles in neurodegenerative diseases: a missing lnc found? *Non-coding RNA Res* 3: 243–252
- An H, Tan JT, Shelkovernikova TA (2019) Stress granules regulate stress-induced paraspeckle assembly. *J Cell Biol* 218: 4127–4140
- Anantharaman A, Jadhaliha M, Tripathi V, Nakagawa S, Hirose T, Jantsch MF, Prasanth SG, Prasanth KV (2016) Paraspeckles modulate the intranuclear distribution of paraspeckle-associated Ctn RNA. *Sci Rep* 6: 34043
- Batsché E, Yaniv M, Muchardt C (2006) The human SWI/SNF subunit Brm is a regulator of alternative splicing. *Nat Struct Mol Biol* 13: 22–29
- Bhattacharya S, Levy MJ, Zhang N, Li H, Florens L, Washburn MP, Workman JL (2021a) The methyltransferase SETD2 couples transcription and splicing by engaging mRNA processing factors through its SH1 domain. *Nat Commun* 12: 1443
- Bhattacharya S, Wang S, Reddy D, Shen S, Zhang Y, Zhang N, Li H, Washburn MP, Florens L, Shi Y et al (2021b) Structural basis of the interaction between SETD2 methyltransferase and hnRNP L paralogs for governing co-transcriptional splicing. *Nat Commun* 12: 6452
- Brownlee PM, Chambers AL, Cloney R, Bianchi A, Downs JA (2014) BAF180 promotes cohesion and prevents genome instability and aneuploidy. *Cell Rep* 6: 973–981
- Butler AA, Johnston DR, Kaur S, Lubin FD (2019) Long noncoding RNA NEAT1 mediates neuronal histone methylation and age-related memory impairment. *Sci Signal* 12: eaaw9277
- Celen C, Chuang J-C, Luo X, Nijem N, Walker AK, Chen F, Zhang S, Chung AS, Nguyen LH, Nassour I et al (2017) Arid1b haploinsufficient mice reveal neuropsychiatric phenotypes and reversible causes of growth impairment. *eLife* 6: e25730
- Chandler Ronald L, Brennan J, Schisler Jonathan C, Serber D, Patterson C, Magnuson T (2013) ARID1a-DNA interactions are required for promoter occupancy by SWI/SNF. *Mol Cell Biol* 33: 265–280
- Choi H, Kim S, Fermin D, Tsou CC, Nesvizhskii AI (2015) QPROT: statistical method for testing differential expression using protein-level intensity data in label-free quantitative proteomics. *J Proteomics* 129: 121–126
- Clemson CM, Hutchinson JN, Sara SA, Ensminger AW, Fox AH, Chess A, Lawrence JB (2009) An architectural role for a nuclear noncoding RNA: NEAT1 RNA is essential for the structure of paraspeckles. *Mol Cell* 33: 717–726
- El Hadidy N, Uversky VN (2019) Intrinsic disorder of the BAF complex: roles in chromatin remodeling and disease development. *Int J Mol Sci* 20: 5260
- Florens L, Washburn MP (2006) Proteomic analysis by multidimensional protein identification technology. *Methods Mol Biol* 328: 159–175
- Flores-Alcantar A, Gonzalez-Sandoval A, Escalante-Alcalde D, Lomeli H (2011) Dynamics of expression of ARID1A and ARID1B subunits in mouse embryos and in cells during the cell cycle. *Cell Tissue Res* 345: 137–148
- Formicola N, Vijayakumar J, Besse F (2019) Neuronal ribonucleoprotein granules: dynamic sensors of localized signals. *Traffic* 20: 639–649
- Fox AH, Lam YW, Leung AK, Lyon CE, Andersen J, Mann M, Lamond AI (2002) Paraspeckles: a novel nuclear domain. *Curr Biol* 12: 13–25
- Fox AH, Bond CS, Lamond AI (2005) P54nrb forms a heterodimer with PSP1 that localizes to paraspeckles in an RNA-dependent manner. *Mol Biol Cell* 16: 5304–5315
- Fox AH, Nakagawa S, Hirose T, Bond CS (2018) Paraspeckles: where long noncoding RNA meets phase separation. *Trends Biochem Sci* 43: 124–135
- Gomes E, Shorter J (2019) The molecular language of membraneless organelles. *J Biol Chem* 294: 7115–7127
- Helming KC, Wang X, Wilson BG, Vazquez F, Haswell JR, Manchester HE, Kim Y, Kryukov GV, Ghandi M, Aguirre AJ et al (2014) ARID1B is a specific vulnerability in ARID1A-mutant cancers. *Nat Med* 20: 251–254
- Hennig S, Kong G, Mannen T, Sadowska A, Kobelke S, Blythe A, Knott GJ, Iyer KS, Ho D, Newcombe EA et al (2015) Prion-like domains in RNA binding proteins are essential for building subnuclear paraspeckles. *J Cell Biol* 210: 529–539
- Hirose T, Virnicchi G, Tanigawa A, Naganuma T, Li R, Kimura H, Yokoi T, Nakagawa S, Bénard M, Fox AH et al (2014) NEAT1 long noncoding RNA regulates transcription via protein sequestration within subnuclear bodies. *Mol Biol Cell* 25: 169–183
- Hirschhorn JN, Brown SA, Clark CD, Winston F (1992) Evidence that SNF2/SWI2 and SNF5 activate transcription in yeast by altering chromatin structure. *Genes Dev* 6: 2288–2298
- Ho L, Ronan JL, Wu J, Staahl BT, Chen L, Kuo A, Lessard J, Nesvizhskii AI, Ranish J, Crabtree GR (2009) An embryonic stem cell chromatin remodeling complex, esBAF, is essential for embryonic stem cell self-renewal and pluripotency. *Proc Natl Acad Sci* 106: 5181–5186
- Huang Y, Li W, Yao X, Lin QJ, Yin JW, Liang Y, Heiner M, Tian B, Hui J, Wang G (2012) Mediator complex regulates alternative mRNA processing via the MED23 subunit. *Mol Cell* 45: 459–469
- Huang J, Ringuet M, Whitten AE, Caria S, Lim YW, Badhan R, Anggono V, Lee M (2020) Structural basis of the zinc-induced cytoplasmic aggregation of the RNA-binding protein SFPQ. *Nucleic Acids Res* 48: 3356–3365
- Hupalowska A, Jedrusik A, Zhu M, Bedford MT, Glover DM, Zernicka-Goetz M (2018) CARM1 and paraspeckles regulate pre-implantation mouse embryo development. *Cell* 175: 1902–1916.e13
- Isobe M, Toya H, Mito M, Chiba T, Asahara H, Hirose T, Nakagawa S (2020) Forced isoform switching of Neat1_1 to Neat1_2 leads to the loss of Neat1_1 and the hyperformation of paraspeckles but does not affect the development and growth of mice. *RNA* 26: 251–264
- Jacq A, Becquet D, Guillen S, Boyer B, Bello-Goutierrez M-M, Franc J-L, François-Bellan A-M (2021) Direct RNA-RNA interaction between Neat1 and RNA targets, as a mechanism for RNAs paraspeckle retention. *RNA Biol* 18: 2016–2027
- Jung E-M, Moffat JJ, Liu J, Dravid SM, Gurumurthy CB, Kim W-Y (2017) Arid1b haploinsufficiency disrupts cortical interneuron development and mouse behavior. *Nat Neurosci* 20: 1694–1707

- Kadoch C, Crabtree GR (2015) Mammalian SWI/SNF chromatin remodeling complexes and cancer: mechanistic insights gained from human genomics. *Sci Adv* 1: e1500447
- Kadoch C, Hargreaves DC, Hodges C, Elias L, Ho L, Ranish J, Crabtree GR (2013) Proteomic and bioinformatic analysis of mammalian SWI/SNF complexes identifies extensive roles in human malignancy. *Nat Genet* 45: 592–601
- Kamelgarn M, Chen J, Kuang L, Jin H, Kasarskis EJ, Zhu H (2018) ALS mutations of FUS suppress protein translation and disrupt the regulation of nonsense-mediated decay. *Proc Natl Acad Sci U S A* 115: E11904–E11913
- Kaneko S, Rozenblatt-Rosen O, Meyerson M, Manley JL (2007) The multifunctional protein p54nrb/PSF recruits the exonuclease XRN2 to facilitate pre-mRNA 3' processing and transcription termination. *Genes Dev* 21: 1779–1789
- Kawaguchi T, Hirose T (2012) Architectural roles of long noncoding RNAs in the intranuclear formation of functional paraspeckles. *Front Biosci* 17: 1729–1746
- Kawaguchi T, Hirose T (2015) Chromatin remodeling complexes in the assembly of long noncoding RNA-dependent nuclear bodies. *Nucleus* 6: 462–467
- Kawaguchi T, Tanigawa A, Naganuma T, Ohkawa Y, Souquere S, Pierron G, Hirose T (2015) SWI/SNF chromatin-remodeling complexes function in noncoding RNA-dependent assembly of nuclear bodies. *Proc Natl Acad Sci U S A* 112: 4304–4309
- Knott GJ, Bond CS, Fox AH (2016) The DBHS proteins SFPQ, NONO and PSPC1: a multipurpose molecular scaffold. *Nucleic Acids Res* 44: 3989–4004
- Kukharsky MS, Ninkina NN, An H, Telezkhin V, Wei W, Meritens CR, Cooper-Knock J, Nakagawa S, Hirose T, Buchman VL et al (2020) Long non-coding RNA Neat1 regulates adaptive behavioural response to stress in mice. *Transl Psychiatry* 10: 171
- Laurent BC, Treitel MA, Carlson M (1991) Functional interdependence of the yeast SNF2, SNF5, and SNF6 proteins in transcriptional activation. *Proc Natl Acad Sci U S A* 88: 2687–2691
- Li K, Wang Z (2021) Speckles and paraspeckles coordinate to regulate HSV-1 genes transcription. *Commun Biol* 4: 1207
- Loo C-S, Gatchalian J, Liang Y, Leblanc M, Xie M, Ho J, Venkatraghavan B, Hargreaves DC, Zheng Y (2020) A genome-wide CRISPR screen reveals a role for the non-canonical nucleosome-remodeling BAF complex in Foxp3 expression and regulatory T cell function. *Immunity* 53: e148
- Macias S, Plass M, Stajuda A, Michlewski G, Eyraes E, Cáceres JF (2012) DGCR8 HITS-CLIP reveals novel functions for the microprocessor. *Nat Struct Mol Biol* 19: 760–766
- Mannen T, Yamashita S, Tomita K, Goshima N, Hirose T (2016) The Sam68 nuclear body is composed of two RNase-sensitive substructures joined by the adaptor HNRNPL. *J Cell Biol* 214: 45–59
- Marnik EA, Updike DL (2019) Membraneless organelles: P granules in *Caenorhabditis elegans*. *Traffic* 20: 373–379
- Mashtalir N, D'Avino AR, Michel BC, Luo J, Pan J, Otto JE, Zullow HJ, McKenzie ZM, Kubiak RL, St. Pierre R et al (2018) Modular organization and assembly of SWI/SNF family chromatin remodeling complexes. *Cell* 175: 1272–1288.e1220
- McDonald WH, Tabb DL, Sadygov RG, MacCoss MJ, Venable J, Graumann J, Johnson JR, Cociorva D, Yates JR 3rd (2004) MS1, MS2, and SQT-three unified, compact, and easily parsed file formats for the storage of shotgun proteomic spectra and identifications. *Rapid Commun Mass Spectrom* 18: 2162–2168
- Michel BC, D'Avino AR, Cassel SH, Mashtalir N, McKenzie ZM, McBride MJ, Valencia AM, Zhou Q, Bocker M, Soares LMM et al (2018) A non-canonical SWI/SNF complex is a synthetic lethal target in cancers driven by BAF complex perturbation. *Nat Cell Biol* 20: 1410–1420
- Naganuma T, Nakagawa S, Tanigawa A, Sasaki YF, Goshima N, Hirose T (2012) Alternative 3'-end processing of long noncoding RNA initiates construction of nuclear paraspeckles. *EMBO J* 31: 4020–4034
- Nagl NG Jr, Patsialou A, Haines DS, Dallas PB, Beck GR Jr, Moran E (2005) The p270 (ARID1A/SMARCF1) subunit of mammalian SWI/SNF-related complexes is essential for normal cell cycle arrest. *Cancer Res* 65: 9236–9244
- Nakagawa S, Naganuma T, Shioi G, Hirose T (2011) Paraspeckles are subpopulation-specific nuclear bodies that are not essential in mice. *J Cell Biol* 193: 31–39
- Nakagawa S, Shimada M, Yanaka K, Mito M, Arai T, Takahashi E, Fujita Y, Fujimori T, Standaert L, Marine JC et al (2014) The lncRNA Neat1 is required for corpus luteum formation and the establishment of pregnancy in a subpopulation of mice. *Development* 141: 4618–4627
- Pagliaroli L, Porazzi P, Curtis AT, Scopa C, Mikkers HMM, Freund C, Daxinger L, Deliard S, Welsh SA, Offley S et al (2021) Inability to switch from ARID1A-BAF to ARID1B-BAF impairs exit from pluripotency and commitment towards neural crest formation in ARID1B-related neurodevelopmental disorders. *Nat Commun* 12: 6469
- Peng R, Dye BT, Pérez I, Barnard DC, Thompson AB, Patton JG (2002) PSF and p54nrb bind a conserved stem in U5 snRNA. *RNA* 8: 1334–1347
- Peterson CL, Herskowitz I (1992) Characterization of the yeast SWI1, SWI2, and SWI3 genes, which encode a global activator of transcription. *Cell* 68: 573–583
- Pisani G, Baron B (2019) Nuclear paraspeckles function in mediating gene regulatory and apoptotic pathways. *Non-coding RNA Res* 4: 128–134
- Pisani G, Baron B (2020) NEAT1 and paraspeckles in cancer development and chemoresistance. *Noncoding RNA* 6: 43
- Porter EG, Dykhuizen EC (2017) Individual bromodomains of polybromo-1 contribute to chromatin association and tumor suppression in clear cell renal carcinoma. *J Biol Chem* 292: 2601–2610
- Prasanth KV, Prasanth SG, Xuan Z, Hearn S, Freier SM, Bennett CF, Zhang MQ, Spector DL (2005) Regulating gene expression through RNA nuclear retention. *Cell* 123: 249–263
- Priam P, Krasteva V, Rousseau P, D'Angelo G, Gaboury L, Sauvageau G, Lessard JA (2017) SMARCD2 subunit of SWI/SNF chromatin-remodeling complexes mediates granulopoiesis through a CEBP ϵ dependent mechanism. *Nat Genet* 49: 753–764
- Raab JR, Resnick S, Magnuson T (2015) Genome-wide transcriptional regulation mediated by biochemically distinct SWI/SNF complexes. *PLoS Genet* 11: e1005748
- Raab JR, Runge JS, Spear CC, Magnuson T (2017) Co-regulation of transcription by BRG1 and BRM, two mutually exclusive SWI/SNF ATPase subunits. *Epigenetics Chromatin* 10: 62
- Raab JR, Smith KN, Spear CC, Manner CJ, Calabrese JM, Magnuson T (2019) SWI/SNF remains localized to chromatin in the presence of SCHLAP1. *Nat Genet* 51: 26–29
- Roberts CWM, Leroux MM, Fleming MD, Orkin SH (2002) Highly penetrant, rapid tumorigenesis through conditional inversion of the tumor suppressor gene Snf5. *Cancer Cell* 2: 415–425
- Sasaki YTF, Ideue T, Sano M, Mituyama T, Hirose T (2009) MENepsilon/beta noncoding RNAs are essential for structural integrity of nuclear paraspeckles. *Proc Natl Acad Sci U S A* 106: 2525–2530
- Shen S, Park JW, Lu Z-x, Lin L, Henry MD, Wu YN, Zhou Q, Xing Y (2014) rMATS: robust and flexible detection of differential alternative splicing from replicate RNA-Seq data. *Proc Natl Acad Sci U S A* 111: E5593–E5601

- Sim JCH, White SM, Lockhart PJ (2015) *ARID1B*—mediated disorders: mutations and possible mechanisms. *Intractable Rare Dis Res* 4: 17–23
- Standaert L, Adriaens C, Radaelli E, Van Keymeulen A, Blanpain C, Hirose T, Nakagawa S, Marine JC (2014) The long noncoding RNA Neat1 is required for mammary gland development and lactation. *RNA* 20: 1844–1849
- Strzyz P (2018) Concentrating on intrinsic disorder. *Nat Rev Genet* 19: 534
- Tabb DL, McDonald WH, Yates JR 3rd (2002) DTASelect and contrast: tools for assembling and comparing protein identifications from shotgun proteomics. *J Proteome Res* 1: 21–26
- Torres M, Becquet D, Blanchard M-P, Guillen S, Boyer B, Moreno M, Franc J-L, François-Bellan A-M (2016) Circadian RNA expression elicited by 3'-UTR IRAlu-paraspeckle associated elements. *eLife* 5: e14837
- Trizzino M, Barbieri E, Petracovici A, Wu S, Welsh SA, Owens TA, Licciulli S, Zhang R, Gardini A (2018) The tumor suppressor ARID1A controls global transcription via pausing of RNA polymerase II. *Cell Rep* 23: 3933–3945
- Tyagi A, Ryme J, Brodin D, Östlund Farrants AK, Visa N (2009) SWI/SNF associates with nascent pre-mRNPs and regulates alternative pre-mRNA processing. *PLoS Genet* 5: e1000470
- Wang X, Nagl NG, Wilsker D, Van Scoy M, Pacchione S, Yaciuk P, Dallas PB, Moran E (2004) Two related ARID family proteins are alternative subunits of human SWI/SNF complexes. *Biochem J* 383: 319–325
- Wang J, Rajbhandari P, Damianov A, Han A, Sallam T, Waki H, Villanueva CJ, Lee SD, Nielsen R, Mandrup S et al (2017) RNA-binding protein PSPC1 promotes the differentiation-dependent nuclear export of adipocyte RNAs. *J Clin Invest* 127: 987–1004
- Wang S, Zuo H, Jin J, Lv W, Xu Z, Fan Y, Zhang J, Zuo B (2019) Long noncoding RNA Neat1 modulates myogenesis by recruiting Ezh2. *Cell Death Dis* 10: 505
- Wang C, Duan Y, Duan G, Wang Q, Zhang K, Deng X, Qian B, Gu J, Ma Z, Zhang S et al (2020) Stress induces dynamic, cytotoxicity-antagonizing TDP-43 nuclear bodies via paraspeckle lncRNA NEAT1-mediated liquid-liquid phase separation. *Mol Cell* 79: 443–458.e7
- West JA, Davis Christopher P, Sunwoo H, Simon Matthew D, Sadreyev Ruslan I, Wang Peggy I, Tolstorukov Michael Y, Kingston Robert E (2014) The long noncoding RNAs NEAT1 and MALAT1 bind active chromatin sites. *Mol Cell* 55: 791–802
- Xu T, Park SK, Venable JD, Wohlschlegel JA, Diedrich JK, Cociorva D, Lu B, Liao L, Hewel J, Han X et al (2015) ProLuCID: an improved SEQUEST-like algorithm with enhanced sensitivity and specificity. *J Proteomics* 129: 16–24
- Yamamoto K, Goyama S, Asada S, Fujino T, Yonezawa T, Sato N, Takeda R, Tsuchiya A, Fukuyama T, Tanaka Y et al (2021) A histone modifier, ASXL1, interacts with NONO and is involved in paraspeckle formation in hematopoietic cells. *Cell Rep* 36: 109576
- Zhang C, Rabouille C (2019) Membrane-bound meet membraneless in health and disease. *Cell* 8: 1000
- Zhang Y, Wen Z, Washburn MP, Florens L (2009) Effect of dynamic exclusion duration on spectral count based quantitative proteomics. *Anal Chem* 81: 6317–6326
- Zhang Y, Wen Z, Washburn MP, Florens L (2010) Refinements to label free proteome quantitation: how to deal with peptides shared by multiple proteins. *Anal Chem* 82: 2272–2281
- Zhang Y, Wen Z, Washburn MP, Florens L (2011) Improving proteomics mass accuracy by dynamic offline lock mass. *Anal Chem* 83: 9344–9351



License: This is an open access article under the terms of the [Creative Commons Attribution-NonCommercial-NoDerivs](https://creativecommons.org/licenses/by-nc-nd/4.0/) License, which permits use and distribution in any medium, provided the original work is properly cited, the use is non-commercial and no modifications or adaptations are made.